J. Fluid Mech. (2007), *vol.* 573, *pp.* 399–415.
doi:10.1017/S0022112006004010 Printed in the United Kingdom

Integral properties of the swash zone and averaging. Part 3. Longshore shoreline boundary conditions for wave-averaged nearshore circulation models

M. ANTUONO, M. BROCCHINI AND G. GROSSO

DIAm, Università di Genova, 16145 Genova, Italy

(Received 20 December 2005 and in revised form 25 August 2006)

The aim of the present work, final of a three-part series, is to analyse in detail flow motions within the swash zone and define suitable shoreline boundary conditions for the longshore flow for wave-averaged circulation models. The analyses of Parts 1 and 2 are extended to cover horizontally two-dimensional flows. An analytical solution for the longshore motion representing the drift velocity of the whole swash zone water mass is found. This is seen to be approximated well by the ratio between the time integral of the longshore momentum flux crossing the swash lower boundary and the swash zone net water volume. Further, a complete set of shoreline boundary conditions, taking into account wave–wave interactions, is obtained on the basis of fully numerical solutions of the nonlinear shallow-water equations. The main focus of the work is to clarify the structure of the shoreline boundary conditions for the longshore flow, but attention has also been paid to their derivation and assessment from the numerical solutions. The latter have been obtained on the basis of a fairly broad range of input wave conditions which, though biased towards those typical of reflective beaches, are believed to cover conditions also typical of moderate dissipative beaches. Two main terms are found to contribute to the longshore drift velocity: (i) a term, proportional to the shallow-water velocity, accounting for short-wave interactions, frictional swash zone forces and continuous forcing due to non-breaking wave nonlinearities and (ii) a drift-type term representing the momentum transfer due to wave breaking.

1. Introduction

Swash zone dynamics deeply influence the surf zone hydro- and morphodynamics (see Elfrink & Baldock 2002 for a detailed review). The role played by such dynamics on the longshore drift and sediment transport is crucial (e.g. Kamphuis 1991; Van Wellen *et al.* 2000). 'The two issues requiring most urgent research attention with regards to swash zone sediment transport processes are the roles of sediment advection and longshore swash motion' (Masselink & Puleo 2006). Moreover swash zone flows are of fundamental importance not only because of their local effects (e.g. structures overtopping, longshore sediment transport, beach and dune erosion, etc.), but also because they influence the surf zone dynamics as a whole (e.g. Russel 1993; Brocchini 2006). For this reason, any models reproducing flow motions in the nearshore should not neglect swash zone dynamics.

However, problems arise because wave-averaged circulation models (averaging over the typical period of wind waves) cannot deal with swash zone flows directly. Often, a pragmatic perspective is taken for which a 'wall boundary', i.e. a perfectly reflecting vertical wall positioned at a given cross-shore location (usually the still-water shoreline) is used. This approach, however, significantly alters the natural flow pattern of seaward-reflected waves (e.g. Brocchini 2006), with an overestimate of the high-frequency content (short waves are fully reflected) and an understimate, of the order of 10%–30%, of the low-frequency content (no wave–wave interaction in the swash zone is allowed for). Hence, the need for suitable shoreline boundary conditions (SBCs) which take into account the presence of the swash zone.

Assumptions made to obtain circulation models, both horizontally two-dimensional (2DH) (e.g. Park & Borthwick 2001) and quasi-three-dimensional (e.g. Van Dongeren & Svendsen 2000), limit their capability to reproduce natural flow conditions which occur at the boundary between the wet and dry domains. It is particularly worrying that the more frequently used simplifications lead to unrealistically weak seaward radiation of low-frequency waves (LFW are waves with periods ranging between 30 s and 300 s) which, in turn, provides an incorrect forcing for the nearshore sediment transport.

If the wet/dry boundary is taken as the intersection of the mean water level with the beach face, both theoretical and practical problems arise: flow integration would occur also during periods of local dry conditions. Even worse would be to average flow properties at the instantaneous shoreline and regard them as swash zone boundary conditions (as for the model by Zhao & Svendsen 2006): not only does the above theoretical problem remain unsolved but no wave–wave interactions, fundamental for a correct energy partitioning of the nearshore flows (e.g. Mase 1995), can be accounted for.

Such interaction is particularly important in the case of reflective beaches on which waves are not so strongly depth limited, it is relatively less important in the case of dissipative beaches over which much of the LFW content is due to standing waves. Hence, if use of suitable SBCs is essential to reproduce frequency downshifting over reflective beaches, it is also important, though less crucial, to establish the correct location of the standing-wave nodal points over dissipative beaches.

Analysis of different definitions for the mean shoreline made by Brocchini & Peregrine (1996), has revealed that such an interface cannot be uniquely defined; but problems can be overcome if the boundary between wet and dry is taken as the *envelope* of the rundown positions, since flow properties can be unambiguously defined in the wet region.

The main aim of our work is to define, along such an envelope, suitable SBCs for wave-averaged circulation models which take into account the proper dynamics of the swash zone. The integral model proposed in Part 1 (Brocchini & Peregrine 1996) is used and the detailed analysis for horizontally one-dimensional flows (1DH) given in Part 2 (Brocchini & Bellotti 2002) and validated through large-scale laboratory experiments by Bellotti, Archetti & Brocchini (2003), is extended to the 2DH case. Such an extension, as well as completing the analysis of the hydrodynamic problem, is of fundamental importance since sediment transport and flow–structure interactions strictly depend on the longshore motion. The main challenge in describing such motion is represented by (i) making use of an appropriate definition of the swash zone drift velocity and (ii) the correct modelling of the continuous forcing of the longshore velocity component caused by nonlinearities and wave breaking.

In § 2, the integral model is extended and clarified for the 2DH case, while § 3 describes an analytical solution for the longshore flow. Closures required for practical applications and the final set of SBCs are proposed in § 4. Conclusions are given in § 5.

2. The integral model

The model we consider makes use of the nonlinear shallow-water equations (NSWE) obtained assuming that vertical accelerations of the water or those normal to the beach are negligible compared with gravity. We introduce basic definitions, choosing the still-water level to be $z = 0$ (z pointing upward), the onshore coordinate x to point landward with $x = 0$ at the still-water shoreline and the total water depth to be

$$d(x, y, t) = h(x, y) + \eta(x, y, t), \tag{2.1}$$

where $z = -h(x, y)$ is the seabed location, $z = \eta(x, y, t)$ is the position of the free surface and y is the longshore coordinate oriented to make with x and z a right-handed Cartesian reference frame. The onshore and longshore velocity components $u(x, y, t)$ and $v(x, y, t)$ are the depth-independent horizontal velocities.

We assume motions to occur over an uniformly plane beach with mild longshore variations. These assumptions, which allow for the use of an analytical treatment of the problem, are not too restrictive for most of the natural swash flow conditions for which beaches are almost planar or piecewise planar (a change of slope may occur near the shoreline at the beginning/end of storms) and waves, rotated by refraction with fronts almost parallel to the shoreline, characterized by a weak longshore variation (see Ryrie's 1983 approximation and also equation (3.1) which follows). Then we can suppose $h_{,x} = \alpha$ and $h_{,y} = 0$ (the notation $(.)_{,i}$ is used for partial differentiation with respect to the variable i). The dimensional general set of equations in conservation form is (see Part 1):

$$d_{,t} + (ud)_{,x} + (vd)_{,y} = 0, \tag{2.2a}$$

$$(ud)_{,t} + \left(u^2 d + \tfrac{1}{2} g d^2\right)_{,x} + (uvd)_{,y} + \alpha g d + \tau_1 = 0, \tag{2.2b}$$

$$(vd)_{,t} + (uvd)_{,x} + \left(v^2 d + \tfrac{1}{2} g d^2\right)_{,y} + \tau_2 = 0, \tag{2.2c}$$

where g is acceleration due to gravity and $\boldsymbol{\tau} = (\tau_1, \tau_2) = (C_f |u| u, C_f |u| v)$ is the bed friction evaluated, in terms of the friction coefficient C_f, on the basis of a steady-flow approach. Although formally more complicated, unsteady approaches are now available (e.g. Nielsen 2002), the typical Chezy-type formulation is shown to provide accurate enough results (e.g. Archetti & Brocchini 2002) and is fairly easily incorporated into the integral swash zone model used in the analysis which follows (e.g. Archetti & Brocchini 2002; Bellotti *et al.* 2003).

When the NSWE are numerically integrated for the surf and swash zone flows, the third equation provides an oscillatory solution with a mean growing, over times longer than typical modulations (e.g. Ryrie 1983), because of nonlinear momentum transfer from the cross-shore to the longshore direction (e.g. Longuet-Higgins 1970). This represents a challenge when replacing the swash zone by a simplified model, capable of providing appropriate SBCs at the seaward swash zone limit for wave-averaged solvers.

In our model, the swash zone limits are x_l (seaward or lower limit) and x_s (instantaneous shoreline, i.e. shoreward or higher limit for integration). The seaward boundary is taken as the lowest limit of the shoreline (see figure 1). The above equations are integrated over the swash zone with the assumption that wave motion evolves on a 'fast time scale' T_s (short-period waves), while the lowest swash zone boundary, x_l (run-down), is supposed to vary on a 'slow time scale' $T_s^{(2)}$ (long-period waves). We identify the 'fast time scale' T_s with the typical period of each single

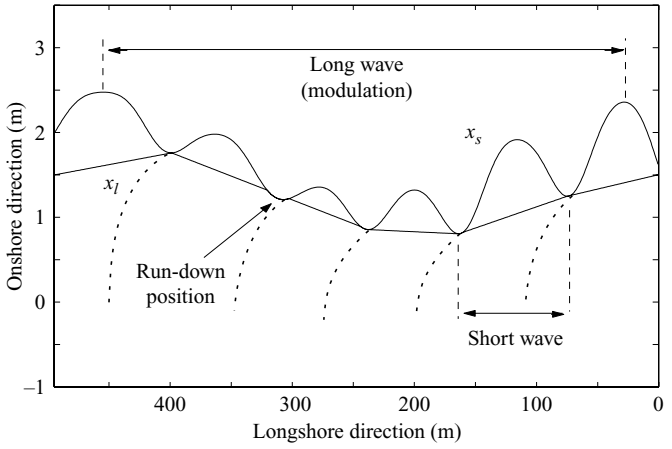

FIGURE 1. Sketch of the flow evolution of the swash zone at a given time ($t = 33$ s). Bimodal waves with offshore wave heights $H_s = 0.17$ m, $H_s^{(2)} = H_s/4$ and periods $T_s = 4.8$ s, $T_s^{(2)} = 5T_s$ evolve over a uniformly sloping beach of slope $\alpha = 0.1$ and with friction coefficient $C_f = 0.01$. The offshore boundary is placed at a depth $d_0 = 1$ m. The instantaneous local shoreline (x_s), the envelope of the rundown positions (x_l) and an indication of the bore paths (thick dashed lines) are illustrated.

incident wave and the 'slow time scale' $T_s^{(2)}$ with the typical period of modulation of incident short waves. In accordance with the assumptions used in Part 1 to formulate the integral swash zone model, seen to reproduce experimental conditions successfully (Bellotti *et al.* 2003), we assume that (Part 1) 'swash motions are almost entirely governed by short-wave contributions and that the only long-wave contribution comes from parameterizing the longshore drift due to wave-breaking by a longshore current velocity $W = W(y, t)$.' Hence, we use the following decomposition:

$$u = \frac{\partial x_l}{\partial t} + \hat{u}, \tag{2.3}$$

where $\hat{u}$ is the cross-shore velocity inside the swash zone.

Since we aim at defining a longshore drift velocity W for the entire swash zone, a slightly different decomposition, which makes use of the spatial average over the swash width, is employed. We thus introduce the swash-averaging operator $M\{.\}$ which applied to the generic function f, leads to:

$$M\{f\} \equiv \frac{1}{x_s - x_l} \int_{x_l}^{x_s} f \, \mathrm{d}x. \tag{2.4}$$

Hence, with a definition similar to that of a Stokes drift-type velocity (e.g. Brocchini 1997), we put

$$v = W + \check{v} \qquad \text{in which} \qquad W \equiv \langle M\{v\} \rangle \quad \text{and} \quad \langle M\{\check{v}\} \rangle = 0, \tag{2.5}$$

in which $\langle\rangle$ indicates the average over the short-period waves. Note that, differently from (2.3), the decomposition in short and long waves of the longshore momentum equation is made after the spatial average over the swash is performed. Hence, the velocity fluctuation $\check{v}$ has to obey an integral constraint as given in (2.5). Moreover, we assume that only W can take into account the action of bores eventually forcing the swash dynamics.

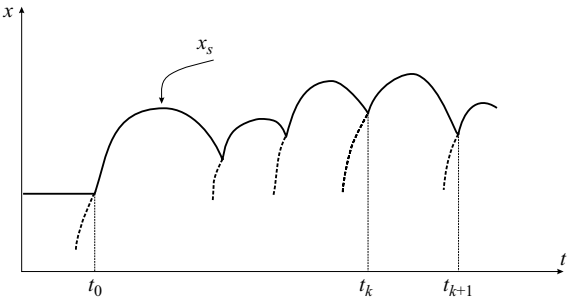

FIGURE 2. Labelling of initial times for individual runups and indication of bore paths (thick dashed lines).

In fact, defining t_k (see figure 2) the kth instant for which $x_s = x_l$, if $|t - t_k| \ll 1$ we can write $x_s = x_l + \varepsilon$ with $\varepsilon \ll 1$ and, consequently, we have:

$$\int_{x_l}^{x_s} f \,\mathrm{d}x = \int_{x_l}^{x_l+\varepsilon} f \,\mathrm{d}x \equiv F(\varepsilon) = F(0) + \frac{\mathrm{d}F}{\mathrm{d}x}(0)\varepsilon + O(\varepsilon^2) \simeq f|_{x_l}(x_s - x_l). \tag{2.6}$$

Using (2.6), it follows that

$$\lim_{t\to t_k} W = \lim_{t\to t_k} \langle M\{v\}\rangle = \langle v(x_s(t_k), y_s(t_k), t_k)\rangle. \tag{2.7}$$

in which y_s indicates the longshore coordinate of the shoreline. Since a bore eventually occurs between two subsequent swashes, from (2.7) we obtain $W \to \langle v_k\rangle^-$ as $t \to (t_k)^-$ and $W \to \langle v_k\rangle^+$ as $t \to (t_k)^+$, so that the jump in the long-period component of the longshore velocity is $[\![\langle v\rangle]\!]_-^+ \equiv \langle v_k\rangle^+ - \langle v_k\rangle^- = [\![W]\!]$. Finally, since we can assume $[\![\langle v\rangle]\!] \simeq [\![v]\!]$, such a result confirms that W can take into account the breaking-induced jump in longshore velocity. Moreover, since the spatial average of $\breve{v}$ represents a short-wave contribution, we assume that all the integral quantities containing $\breve{v}$ represent short-wave terms. Note that definition (2.5) of W, notwithstanding its simplicity, cannot explicitly express the main contributions we are searching for: the local instantaneous forcing due to nonlinearities and the periodic momentum transfer due to wave breaking.

In order to have a clear decomposition of the flow dynamics, we substitute (2.3) and (2.5) into the equation of longshore momentum (see Part 1 for more details on the derivation of the integral equations), obtaining:

$$\frac{\partial\langle WV\rangle}{\partial t} + \frac{\partial\langle \breve{P}_2\rangle}{\partial t} + \frac{\partial\langle W^2V\rangle}{\partial y} + 2\frac{\partial\langle W\breve{P}_2\rangle}{\partial y} + \frac{\partial\langle \breve{M}_{22}\rangle}{\partial y} + \langle \Upsilon_2\rangle = \left[\left\langle\left(u - \frac{\partial x_l}{\partial t}\right) vd\right\rangle\right]_{x_l}$$
$$= \left(\langle u\rangle - \frac{\partial x_l}{\partial t}\right)\langle v\rangle\langle d\rangle + \langle\tilde{u}\tilde{v}\rangle\langle d\rangle + \langle\tilde{u}\tilde{d}\rangle\langle v\rangle + \langle\tilde{v}\tilde{d}\rangle\left(\langle u\rangle - \frac{\partial x_l}{\partial t}\right) + \langle\tilde{u}\tilde{v}\tilde{d}\rangle, \tag{2.8}$$

where

$$V \equiv \int_{x_l}^{x_h} d \,\mathrm{d}x, \qquad \Upsilon_2 \equiv \int_{x_l}^{x_h} \tau_2 \,\mathrm{d}x, \tag{2.9}$$

$$\breve{P}_2 \equiv \int_{x_l}^{x_h} (\breve{v}d) \,\mathrm{d}x, \qquad \breve{M}_{22} \equiv \int_{x_l}^{x_h} \left(\breve{v}^2 d + \tfrac{1}{2}gd^2\right) \mathrm{d}x, \tag{2.10}$$

C_f	T_s(s)	H_s(m)	θ(deg.)
0.01	3.2*	0.10	4
0.03	4.8◇	0.14	6
0.05	6.4	0.17	8
0.07		0.20	10
		0.23	

TABLE 1. Input parameters used to obtain the fully numerical NSWE solutions used to assess the value of the model equations. T_s and H_s are the short-wave period and height, θ is the angle of incidence to the beach normal of the waves evaluated at the seaward boundary of the sloping region, C_f is the frictional coefficient. The period indicated by '*' is used only for JONSWAP spectra, while that indicated by '◇' only for bimodal waves.

and the following short/long wave decomposition is used seaward of x_l, i.e. in the inner surf zone:

$$u = \langle u \rangle + \widetilde{u}, \quad v = \langle v \rangle + \widetilde{v}, \quad d = \langle d \rangle + \widetilde{d}, \quad \langle \widetilde{u} \rangle = \langle \widetilde{v} \rangle = \langle \widetilde{d} \rangle = 0. \tag{2.11}$$

Evaluation of the integral model (see Parts 1 and 2) is made on the basis of fully numerical solutions of the 2DH NSWE (2.2), i.e. inclusive of the longshore flow propagation, computed with the shock-capturing solver of Brocchini *et al.* (2001). Such a solver, implementing accurate shoreline boundary conditions (see their §4) based on the appropriate solution of a wet/dry Riemann problem, provides an accurate description of swash zone flows, essential for the analyses which follow. In this respect, a numerical discretization has been used such that the swash zone width is always discretized with at least 10 grid points. To clearly assess the value of the above model equation, we use, as in Part 2, either irregular waves obtained through a JONSWAP spectrum and bimodal waves to check the balance between the left-hand side and the right-hand side of (2.8).

For such an initial analysis (others follow in §4 for the model calibration and final evaluation), we used an uniformly sloping beach of slope $\alpha = 0.1$ and a Froude-type scaling was considered, resulting in the input data of table 1. The input wave values, chosen also in view of feasible NSWE simulations (i.e. waves not too steep at the offshore boundary), cover a rather broad range of natural conditions: for a 1:7 geometric scaling to prototype, we find $8\,\mathrm{s} \leqslant T_s \leqslant 17\,\mathrm{s}$ and $0.7\,\mathrm{m} \leqslant H_s \leqslant 1.5\,\mathrm{m}$. Moreover, they closely match typical input wave conditions used in experimental analyses both of specific swash zone phenomena (e.g. Baldock *et al.* 2005) and of overall nearshore hydro-morpho-dynamics (e.g. Wang *et al.* 2002).

In the case of JONSWAP spectra, T_s and H_s are the short-wave significant period (about 0.78 of the peak period) and height; for regular waves, $T_s \equiv T$ and $H_s \equiv H$ are the short-wave period and height; whereas for bimodal waves, modulations were obtained by the interaction of the short wave with a secondary signal $(H_s^{(2)}, T_s^{(2)}) = (0.25H_s, 5T_s)$. Longshore flow components are forced by varying the incidence angle θ of unidirectional waves at the offshore boundary over the range reported in table 1. Incident waves evolve over a wide computational domain in the longshore direction and open lateral boundary conditions are used. Also note that in the cases forced by regular waves (see analysis of §4), periodicity is established after 3–4 short-wavelengths at most.

In summary, a total of 80 numerical solutions for regular waves, 20 for JONSWAP spectra and 5 for bimodal waves have been used for the comparative analysis which

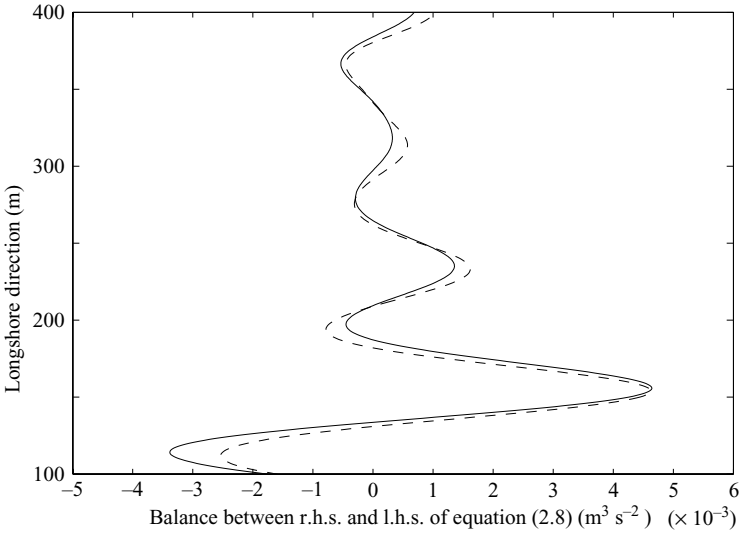

FIGURE 3. The balance between the left-hand side (solid line) and the right-hand side (dashed line) of equation (2.8). The longshore momentum growth due to wave breaking is evident. Flow conditions are described in the caption to figure 1.

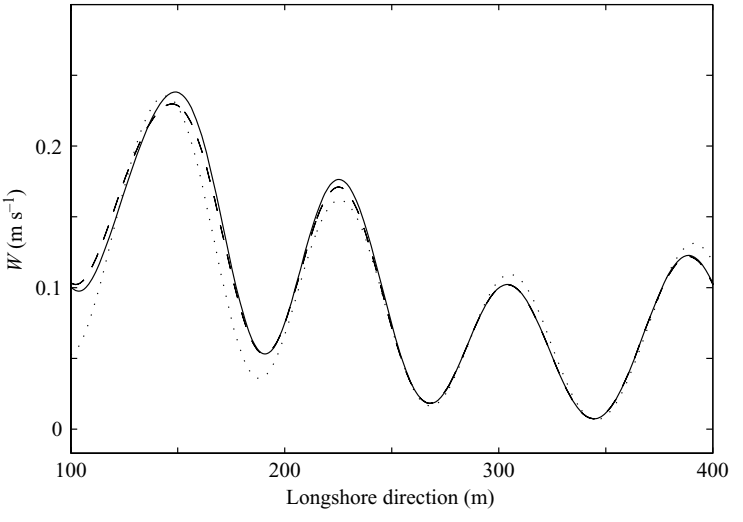

FIGURE 4. Drift velocity comparisons. The numerical solution (2.5) is illustrated by the dotted line while the exact solution (3.9) and the approximate one (3.11) are given, respectively, by the solid and dashed lines. The growth of W due to wave breaking is evident. Flow conditions are described in the caption to figure 1.

follows, and, based on simulations, run for a time sufficiently long to remove any influence of the initial transient (i.e. approximately $15T_s$).

Figure 3 shows a typical example of the left-hand side/right-hand side balance evaluation. Since one-sided computations of derivatives with finite differences at boundaries lead to errors larger than those evaluated at the interior of the domain, it is always useful to discard boundary points in comparisons. Hence, the reduced longshore domain of figures 3 and 4. Also note that, since we compute only first-order

derivatives, the errors made near the boundaries do not propagate to the interior points (subsequent derivatives make use of the function and not of its derivative). The aperiodic shape of the signals, in the chosen longshore window, is due to the interaction within the domain of short and long waves while differences between the two signals are due to: (i) one theoretical cause, i.e. the required parameterization of some contributions appearing at the left-hand side (e.g. $\langle \Upsilon_2 \rangle$) in terms of the model variables; and (ii) the numerical discretization used to obtain the fully numerical solutions. Although the latter can be, in principle, reduced by decreasing the grid size, the former is unavoidable as it is intrinsic to the model. Since average differences are in the order of a few per cent, it seems clear that (2.8) provides a good starting point for defining the longshore SBCs which follow.

3. An analytical solution for the longshore motion

Analysing in detail equation (2.8) we extend the results of Part 2 to the case of weakly 2DH motion. We introduce Ryrie's (1983) approximation by considering waves incident at the seaward boundary of the sloping region with a small angle θ to the beach normal.

Since waves approaching a beach from deep waters are refracted towards the shore, so that θ becomes quite small, the above restriction is not too severe. We, thus, introduce a pseudotime t' and a small parameter ϵ such that

$$t' = t - \epsilon y, \tag{3.1}$$

and assume that this is the only y-dependence for the flow. For example, this occurs for a regular train of waves approaching the beach at an angle θ with the shore normal, with an offshore velocity c, where $\epsilon = \sin(\theta)/c$ (constant by Snell's law) and c is the shallow-water wave velocity $\sqrt{gd}$. This kind of approach can be extended to any beach that has a weakly-varying topography in the longshore direction. Use of (3.1) into (2.8) leads to:

$$\frac{\mathrm{d}}{\mathrm{d}t'}[W\langle V\rangle + \langle \check{P}_2\rangle - \epsilon W^2\langle V\rangle - 2\epsilon W\langle \check{P}_2\rangle - \epsilon\langle \check{M}_{22}\rangle] = \left\langle \left(u - \frac{\partial x_l}{\partial t}\right) vd\big|_{x_l} \right\rangle - \langle \Upsilon_2\rangle. \tag{3.2}$$

For the sake of brevity, we rewrite (3.2) in the following compact form:

$$\frac{\mathrm{d}}{\mathrm{d}t'} P_W(t') = \mathfrak{B}(t') \quad \Rightarrow \quad P_W(t') - P_W(t'_0) = \int_{t'_0}^{t'} \mathfrak{B}(\tau')\,\mathrm{d}\tau' \tag{3.3}$$

in which:

$$P_W(t') \equiv [W\langle V\rangle + \langle \check{P}_2\rangle - \epsilon W^2\langle V\rangle - 2\epsilon W\langle \check{P}_2\rangle - \epsilon\langle \check{M}_{22}\rangle], \tag{3.4}$$

$$\mathfrak{B}(t') \equiv \left\langle \left(u - \frac{\partial x_l}{\partial t}\right) vd\Big|_{x_l} \right\rangle - \langle \Upsilon_2\rangle. \tag{3.5}$$

We denote the time of the beginning of the first run-up as t'_0 and the time at which the kth swash ends as t'_k (see also figure 2). At such instants, $x_s = x_l$, and so all the integral quantities vanish. In particular,

$$P_W(t'_k) = 0 \quad \forall k \in \mathbb{N} \quad \Rightarrow \quad P_W(t'_0) = -\int_{t'_0}^{t'_k} \mathfrak{B}(\tau')\,\mathrm{d}\tau' \quad \forall k \in \mathbb{N}. \tag{3.6}$$

Substituting this result into (3.3), we obtain

$$P_W(t') = \int_{t'_k}^{t'} \mathfrak{B}(\tau')\,\mathrm{d}\tau' \qquad \forall k \in \mathbb{N}, \tag{3.7}$$

and with the usual independent variables (t, y), this can be rewritten in the form:

$$P_W(t, y) = \int_{t_k(y)}^{t} \mathfrak{B}(\tau, y)\,\mathrm{d}\tau \qquad \forall k \in \mathbb{N} \qquad \text{with} \quad t_k(y) = t'_k + \epsilon y. \tag{3.8}$$

The general solution of (3.2), which, as shown in figure 4, compares well with definition (2.5) directly evaluated from the numerical data, is:

$$W = \frac{b - \sqrt{b^2 - 4aC}}{2a}, \tag{3.9}$$

in which:

$$a \equiv \epsilon\langle V\rangle, \quad b \equiv \langle V\rangle - 2\epsilon\langle \check{P}_2\rangle, \quad C \equiv \int_{t_k(y)}^{t} \mathfrak{B}(\tau, y)\,\mathrm{d}\tau + \epsilon\langle \check{M}_{22}\rangle - \langle \check{P}_2\rangle. \tag{3.10}$$

The other root is not taken into account as it is physically meaningless.
Since $\epsilon \ll 1$, we can use the approximate solution $W \cong C/b$. Analysis of the fully numerical solutions described in § 2 shows that the term $\epsilon\langle \check{M}_{22}\rangle$ is negligible (less that 5% of C), i.e.

$$W \cong \frac{\displaystyle\int_{t_k(y)}^{t} \mathfrak{B}(\tau, y)\,\mathrm{d}\tau - \langle \check{P}_2\rangle}{\langle V\rangle}. \tag{3.11}$$

As shown in figure 4, this approximated solution agrees very well with the exact solution (3.9) and, consequently, with the numerically evaluated definition (2.5). Moreover (3.11) confirms our initial inference on the physical meaning of W. In fact, the numerator is an 'effective water mass flux' within the swash zone, while the denominator represents the whole water mass of the swash zone itself. Hence, such a ratio is clearly the drift velocity of the whole water mass (volume) in the swash zone and W can be correctly regarded as the longshore current which represents it.

Definition (2.5) and the analytical exact (3.9) and approximated (3.11) solutions to the longshore problem have all an important role in the following analyses which lead to the SBCs for the longshore flow. In more detail, the analytical solutions (3.9) and (3.11) are used to identify the structure of W and, subsequently, define suitable forms for the required regressions (see § 4) which are obtained by directly using the results of the chosen numerical solutions which also provide (2.5). In this respect, the comparison of figure 4 validates the final SBCs, built with the structure of (3.9) and (3.11), but required to represent the numerically evaluated definition (2.5).

4. Closures and shoreline boundary conditions

In this section, we further elaborate the approximate solution (3.11) to find suitable SBCs for the longshore motion to be implemented in available circulation models. We want to express the integral quantities defined in the swash zone as functions of long-wave properties calculated at x_l. Through the relations obtained, we are able to assign the appropriate SBCs from knowledge of the integral quantities in the swash

and local wave properties. We first recall the results of Part 2:

$$\langle V\rangle \equiv \int_{x_l}^{x_h} d\,\mathrm{d}x \approx C_V H_l^2/\alpha \qquad \text{with} \quad C_V = 0.615 - 0.201 C_f/\alpha, \tag{4.1a}$$

$$\langle \tilde{Q}_1\rangle \equiv \langle \tilde{u}\tilde{d}\rangle \approx C_{Q_1}\sqrt{gH_l^3} \quad \text{with} \quad C_{Q_1} = 0.356 - 0.273\sqrt{C_f/\alpha}, \tag{4.1b}$$

$$\langle \tilde{S}_{11}\rangle \equiv \left\langle \tilde{u}^2 d + \tfrac{1}{2} g \tilde{d}^2\right\rangle \approx C_{S_{11}} g H_l^2 \quad \text{with} \quad C_{S_{11}} = 0.792 - 0.574\sqrt{C_f/\alpha}, \tag{4.1c}$$

$$\langle \Upsilon_1\rangle \equiv \int_{x_l}^{x_h} \tau_1\,\mathrm{d}x \approx C_{\Upsilon_1} g H_l^2 \qquad \text{with} \quad C_{\Upsilon_1} = -0.034\, C_f/\alpha. \tag{4.1d}$$

Such relations are obtained using periodic input conditions and averaging $\langle V\rangle, \langle \tilde{Q}_1\rangle, \langle \tilde{S}_{11}\rangle, \langle \Upsilon_1\rangle$ over single swash events, while H_l is the *local* (i.e. at x_l) wave height. The same procedure is used in the following to obtain the regressions for the 2DH case. We introduce standard variables, which are commonly used in circulation models, as follows:

$$\bar{d} \equiv \langle d\rangle, \qquad \bar{u} \equiv \langle u\rangle + \frac{\langle \tilde{u}\tilde{d}\rangle}{\langle d\rangle}, \qquad \bar{v} \equiv \langle v\rangle + \frac{\langle \tilde{v}\tilde{d}\rangle}{\langle d\rangle}. \tag{4.2}$$

Finally, from Part 2, we have that, once the incoming characteristic variable $\mathscr{R}_+ = \bar{u} + 2\sqrt{\bar{d}}$ is known, the SBCs for 1DH flows are:

$$\bar{d}(x_l) \approx \frac{H_l}{2}, \quad \bar{u}(x_l) \approx \mathscr{R}_+ - \sqrt{2gH_l}, \quad \frac{\mathrm{d}x_l}{\mathrm{d}t} \approx \left(\bar{u} - \frac{2}{H_l}\frac{\mathrm{d}\langle V\rangle}{\mathrm{d}t}\right)\Bigg|_{x_l}. \tag{4.3a–c}$$

By analogy with (4.2) and using Buckingham's theorem for dimensional analysis, we assume the following relations:

$$|\langle \check{P}_2\rangle| \equiv \left|\left\langle \int_{x_l}^{x_h} (\check{v} d)\,\mathrm{d}x \right\rangle\right| \approx C_{P_2}\sqrt{g}/\alpha \sin(\theta) H_l^{5/2}, \tag{4.4a}$$

$$\langle \check{M}_{22}\rangle \equiv \left\langle \int_{x_l}^{x_h} \left(\check{v}^2 d + \tfrac{1}{2} g d^2\right)\mathrm{d}x \right\rangle \approx C_{M_{22}} g/\alpha H_l^3, \tag{4.4b}$$

$$\langle \tilde{Q}_2\rangle \equiv \langle \tilde{v}\tilde{d}\rangle \approx C_{Q_2}\sqrt{g}\sin(\theta) H_l^{3/2}, \tag{4.4c}$$

$$\langle \tilde{S}_{12}\rangle \equiv \langle \tilde{u}\tilde{v}\tilde{d}\rangle \approx C_{S_{12}} g \sin(\theta) H_l^2, \tag{4.4d}$$

$$\langle \Upsilon_2\rangle \equiv \left\langle \int_{x_l}^{x_h} \tau_2\,\mathrm{d}x \right\rangle \approx C_{\Upsilon_2} g \sin(\theta) H_l^2, \tag{4.4e}$$

in which the extra dependence from the angle of wave incidence θ appears with respect to relationships (4.1). Note that since $\langle \check{P}_2\rangle$ does not have a defined sign, we have made the regression of its absolute value. Defining the time scale $t_0 = \alpha^{-1}\sqrt{d_0/g}$ and the dimensionless period $T_s^* = T_s/t_0$, we assume the coefficients of (4.4*a*)–(4.4*e*) to depend both on C_f and T_s^*.

Fitting a fairly large number (64) of fully numerical solutions obtained with periodic input conditions (see table 2), we obtain the following structure for the regression of the coefficients above (see figure 5 where, given the very similar regression behaviours for all periods, only results for the smallest and largest periods in use are shown):

$$C_{(\ldots)} = \frac{a_2 T_s^{*2} + a_1 T_s^* + a_0}{C_f} + \left(b_2 T_s^{*2} + b_1 T_s^* + b_0\right) + C_f\left(c_2 T_s^{*2} + c_1 T_s^* + c_0\right). \tag{4.5}$$

C_f	T_s(s)	H_s(m)	θ(deg.)
0.01	3.2	0.17	6
0.03	4.0	0.23	10
0.05	4.8		
0.07	6.4		

TABLE 2. Input parameters used to obtain fully–numerical periodic NSWE solutions required for the calibration analysis. Definitions as for the caption to table 1.

Note that the dependence on $1/C_f$ is foreseen by Ryrie's work (1983) on periodic breaking waves. We also emphasize that this formulation is valid only when the longshore flow has reached a quasi–steady state (e.g. Ryrie 1983).

For C_{P_2} we obtain:

$$a_2 = 3.7031 \times 10^{-4}, \quad a_1 = -1.4087 \times 10^{-3}, \quad a_0 = 2.1327 \times 10^{-3},$$
$$b_2 = 0.6423 \times 10^{-3}, \quad b_1 = 0.3457 \times 10^{-3}, \quad b_0 = -1.9759 \times 10^{-2},$$
$$c_2 = 1.7226 \times 10^{-2}, \quad c_1 = 2.5289 \times 10^{-2}, \quad c_0 = 6.0260 \times 10^{-2},$$

for $C_{M_{22}}$:

$$a_2 = -0.1515 \times 10^{-2}, \quad a_1 = 0.4325 \times 10^{-2}, \quad a_0 = -0.1327 \times 10^{-2},$$
$$b_2 = 1.9429 \times 10^{-2}, \quad b_1 = -4.098 \times 10^{-2}, \quad b_0 = 5.1766 \times 10^{-2},$$
$$c_2 = -0.3540, \quad c_1 = 1.1203, \quad c_0 = -0.7790,$$

for C_{Q_2}:

$$a_2 = 0.1363 \times 10^{-5}, \quad a_1 = -1.7141 \times 10^{-4}, \quad a_0 = 4.9529 \times 10^{-4},$$
$$b_2 = 0.2691 \times 10^{-2}, \quad b_1 = 0.7012 \times 10^{-2}, \quad b_0 = -1.2511 \times 10^{-2},$$
$$c_2 = -8.5690 \times 10^{-2}, \quad c_1 = 1.3648 \times 10^{-1}, \quad c_0 = 0.1912 \times 10^{-2},$$

for $C_{S_{12}}$:

$$a_2 = -0.1017 \times 10^{-3}, \quad a_1 = 0.3038 \times 10^{-3}, \quad a_0 = 0.2470 \times 10^{-4},$$
$$b_2 = 0.1240 \times 10^{-1}, \quad b_1 = -0.3870 \times 10^{-1}, \quad b_0 = 0.2970 \times 10^{-1},$$
$$c_2 = -0.1079, \quad c_1 = 0.3329, \quad c_0 = -0.2497,$$

and for C_{Υ_2}:

$$a_2 = -0.4191 \times 10^{-3}, \quad a_1 = 1.3129 \times 10^{-3}, \quad a_0 = -0.2509 \times 10^{-3},$$
$$b_2 = 2.1849 \times 10^{-2}, \quad b_1 = -5.8091 \times 10^{-2}, \quad b_0 = 4.4079 \times 10^{-2},$$
$$c_2 = -0.1513, \quad c_1 = 0.3673, \quad c_0 = -0.2244.$$

The moderate scatter observed in figure 5 (more evident for small values of C_f) and in the two following figures reflects the use of different wave conditions.

Now using (4.2), we can expand to its main contributions the longshore momentum flux appearing in $\mathfrak{B}(t)$ (see also equation (3.5)):

$$\left\langle \left(u - \frac{\partial x_l}{\partial t} \right) v d \Big|_{x_l} \right\rangle = \left[\left(\overline{u} - \frac{\partial x_l}{\partial t} \right) \overline{v}\overline{d} - \frac{\langle \tilde{Q}_1 \rangle \langle \tilde{Q}_2 \rangle}{\overline{d}} + \langle \tilde{S}_{12} \rangle + \langle \tilde{u}\tilde{v} \rangle \overline{d} \right] \Bigg|_{x_l}. \tag{4.6}$$

So, defining the time scale $\alpha^{-1}\sqrt{H_l/g}$, which is proportional to the natural swash period $T_{swash} = \sqrt{g H_l}/g\alpha$ (e.g. Baldock & Holmes 1999), using (4.3) and the regressions

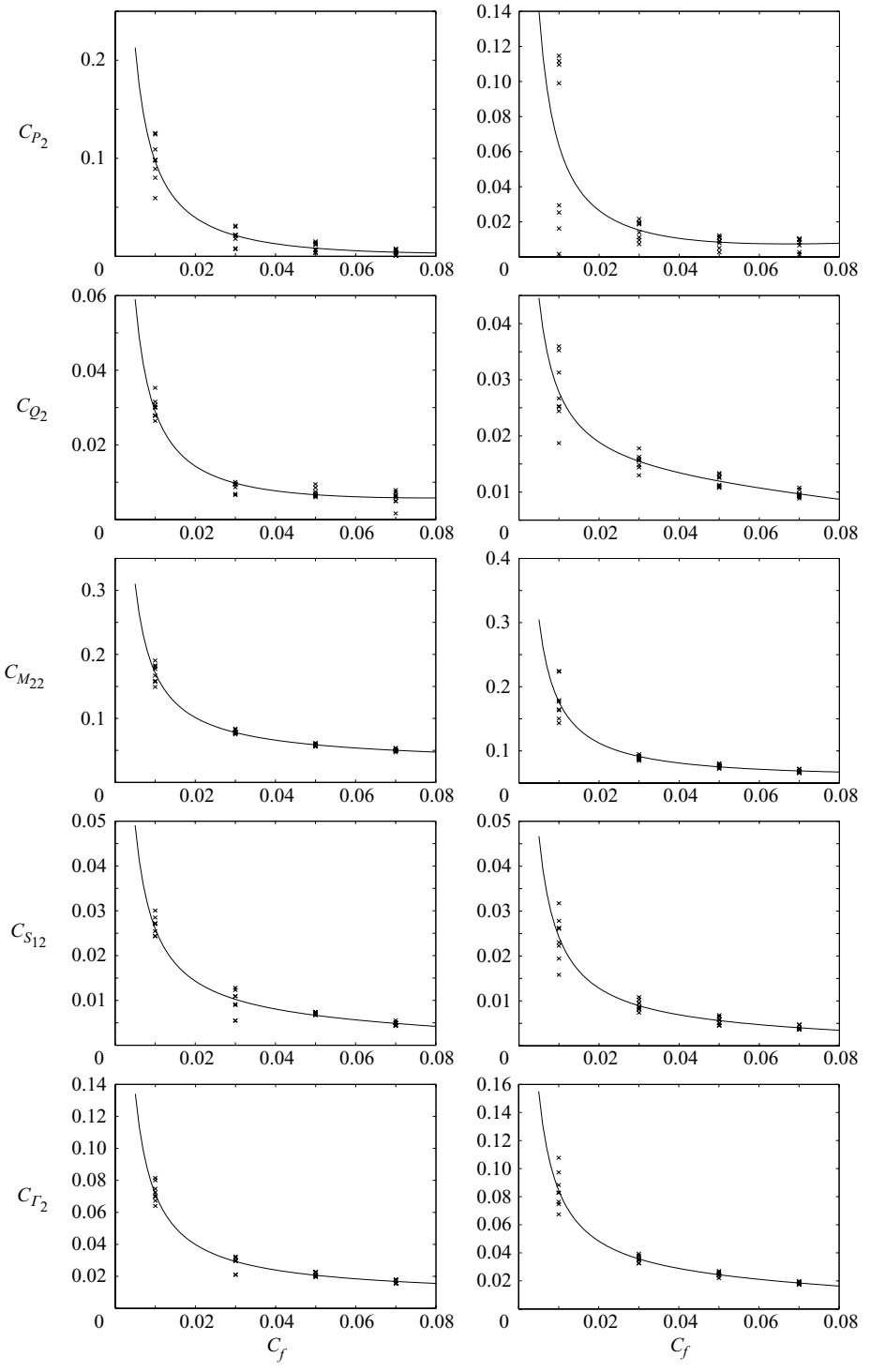

FIGURE 5. Fitting of short-wave properties. Left-hand and right-hand columns correspond to the smallest and largest periods in use $T_s = 3.2\,\mathrm{s}, 6.4\,\mathrm{s}$. Along each row are plotted the regressions curves and the numerically computed data of coefficients $C_{P_2}, C_{Q_2}, C_{M_{22}}, C_{S_{12}}, C_{\Gamma_2}$ of equations (4.4) as functions of C_f.

in (4.4), we assume that (see also Appendix):

$$\int_{t_k(y)}^{t} \mathfrak{B}(\tau, y)\,\mathrm{d}\tau \;\approx\; \frac{H_l^2}{\alpha}[C_1\bar{\bar{v}} + C_2\sin(\theta)\sqrt{gH_l}], \tag{4.7}$$

where the first contribution models the mean momentum flux across x_l while the second models all the short-wave interactions and the frictional forces in the swash zone. Here, C_1 and C_2 are constants while $\bar{\bar{v}}$ is the mean value of $\overline{v}$ at x_l for the single swash at hand:

$$\bar{\bar{v}} \;\equiv\; \frac{1}{t'_{k+1} - t'_k}\int_{t'_k}^{t'_{k+1}} \overline{v}\Big|_{x_l}\,\mathrm{d}\tau'. \tag{4.8}$$

Definition (4.8) is introduced, in analogy with Ryrie (1983), to use a single variable for each swash which can take into account breaking events. Since a bore implies a growth of v from each swash to the following one, $\bar{\bar{v}}$ can, implicitly, account for the jump in longshore velocity $[\![v]\!]$ and also allows us to clarify the dependence of the drift W on such forcing. In fact, substituting (4.7) into (3.11) and using the previous regressions, we obtain the following theoretical form of dependence for W:

$$W \approx [\widetilde{C}_1\bar{\bar{v}} + \widetilde{C}_2\sin(\theta)\sqrt{gH_l}]. \tag{4.9}$$

The final step is to make the dependence of $\bar{\bar{v}}$ on H_l explicit. Since bore generation is most frequent in shallow waters, we want to isolate the contribution due to breaking. Following the approach used by Ryrie (1983) to analyse periodic breaking waves at the shoreline, we assume the following relation for $\bar{\bar{v}}$:

$$\bar{\bar{v}} \approx \left[D_1 + \frac{D_2}{C_f}\frac{T_{swash}}{T_s}\right]\sin(\theta)\sqrt{gH_l}. \tag{4.10}$$

Here D_1 models the purely non-breaking nonlinear contributions to W while the second term represents the contribution due to breaking. The term $\bar{\bar{v}}$ is unbounded as C_f goes to zero which is in good agreement with Ryrie's (1983) results. Substituting (4.10) into (4.9) we obtain the final expression for W:

$$W \approx \left[A + \frac{B}{C_f}\frac{T_{swash}}{T_s}\right]\sin(\theta)\sqrt{gH_l}. \tag{4.11}$$

The best-fitting coefficients are:

$$A = 187.9467C_f^2 - 23.4849C_f + 0.7939, \qquad B = 4.9438C_f^2 - 0.1512C_f + 0.0239,$$

and have been derived from the fitting curves reported on figure 6 where, like for figure 5, the data scatter reduces for increasing C_f.

Equation (4.11) clearly shows the dependence of the drift velocity W on the expected fraction of the local shallow-water velocity (i.e. $\sin(\theta)\sqrt{gH}$) through: a first term (A) which accounts for short-wave interactions, frictional swash zone forces, the purely non-breaking nonlinear contributions and a second term (depending on B) which models breaking forcings.

Evaluation of the performance of the proposed SBCs is given on the basis of further numerical solutions of the NSWE. These have been run on purpose with input values different from those used during both the preliminary assessment of the integral model performances (table 1) and the calibration of the model (table 2). Table 3 summarizes the input values used for the final analysis of the SBCs' assessment.

Figure 7 shows that equation (4.11) predicts well the numerically computed longshore velocity for both monochromatic waves (figure 7*a*) and bimodal waves

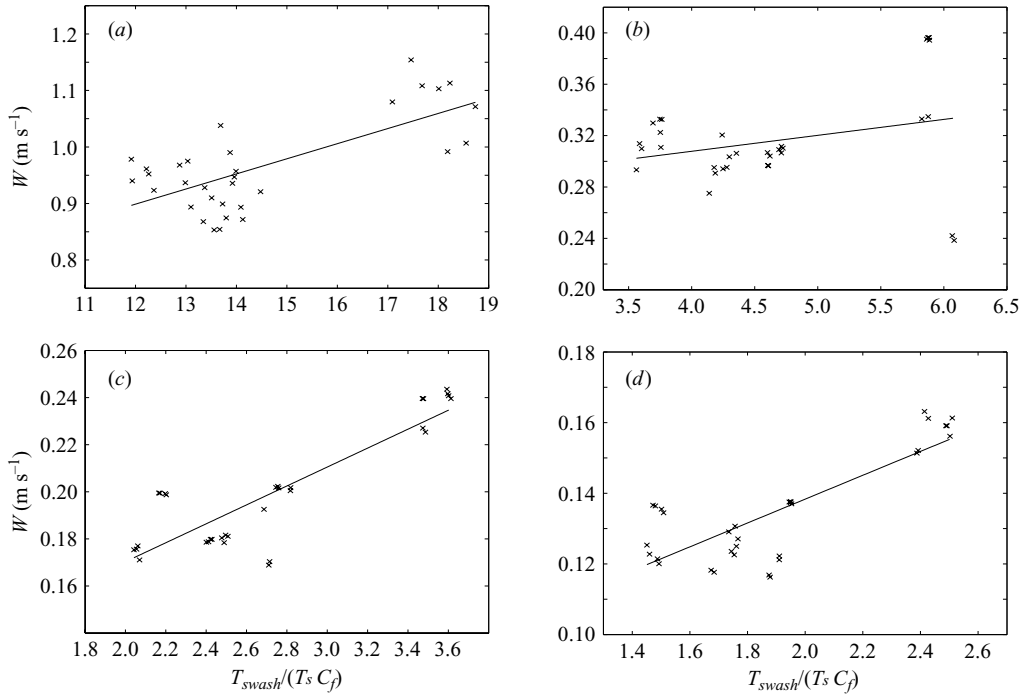

FIGURE 6. Fitting with (4.11) of the numerically computed values of W (see table 2) as a function of $T_{swash}/(T_s C_f)$ with: (*a*) $C_f = 0.01$, (*b*) $C_f = 0.03$, (*c*) $C_f = 0.05$, (*d*) $C_f = 0.07$.

C_f	T_s(s)	H_s(m)	θ(deg.)
0.02	4.8	0.10	6
0.04	4.8°	0.14	
		0.17	
		0.20	
		0.23	

TABLE 3. Input parameters used to obtain the fully numerical NSWE solutions used to assess the value of the proposed SBCs. Definitions as in the caption to table 1.

(figure 7*b*). The moderate overprediction (about 10%–20%) given by (4.11) for the smaller friction coefficient ($C_f = 0.02$) becomes an almost perfect coincidence, for increasing values of the friction coefficient ($C_f = 0.04$). Such improvement seems to reflect the better fits obtained for all the coefficients which require calibration (see figure 5 and 6) for large values of C_f.

In summary, a simple 'recipe' is suggested to prescribe the SBCs. The motion of the mean shoreline is given by (4.3*c*) in which the rate of change of the volume in the swash zone, related to H_l through equation (4.1*a*), acts to decelerate the shoreline motion during the run-up and accelerate it during the run-down. At the mean shoreline, the mean water depth is computed to be about half of H_l (equation 4.3*a*). The onshore velocity depends on both local (H_l) and global information ($\mathscr{R}_+$ coming from the interior of the domain brings to the shoreline knowledge of the deeper water dynamics). Finally, the local longshore velocity is a function of the incident wave angle θ and period T_s beyond the local wave height ($T_{swash} = \sqrt{gH_l}/g\alpha$).

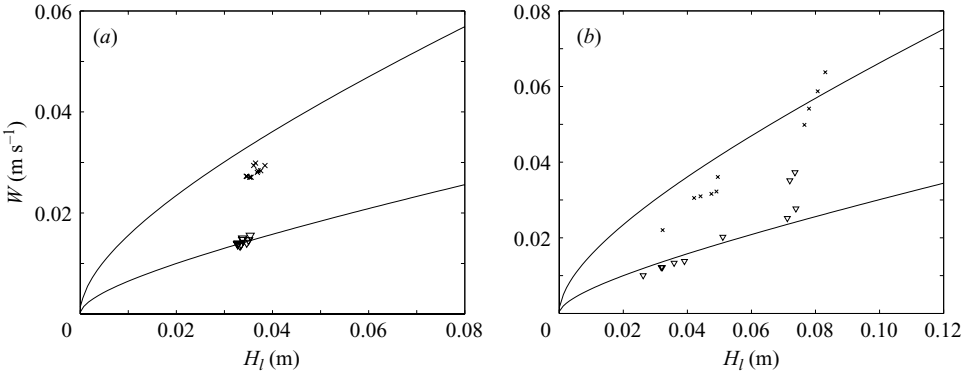

FIGURE 7. Assessment of the predictive capacity of solution (4.11) through a comparison with the numerically computed values of W for the waves of table 3: (*a*) monochromatic waves, (*b*) bimodal waves. x, $C_f = 0.02$; ∇, $C_f = 0.04$.

As anticipated in Part 2, an accurate computation of $\mathscr{R}_+$ at x_l seems to be the most crucial issue in correctly predicting the motion of the mean shoreline from a numerical point of view. Specific problems concerned with the numerical implementation of the full SBCs (comprehensive of the lonshore motion) are still not known as such full implementation is still underway.

5. Conclusions

Complete SBCs for wave-averaged 2DH circulation models have been derived on the basis of an integral version of the NSWE which naturally accounts for the interactions of long and short waves near the shoreline. The integral model can be used to provide SBCs for the longshore drift velocity W only if short-wave contributions are suitably closed. For this purpose and to clarify the dependence of W on the short-wave properties we have:

(*a*) obtained an analytical solution for the longshore drift velocity of the swash zone water masses;

(*b*) computed short-wave contributions by wave-averaging fully numerical solutions of the wave-resolved NSWE, the latter being evaluated with an accuracy sufficient to resolve swash zone flows well.

Contributions to the drift velocity, coming from both nonlinear wave–wave interaction and wave breaking, are written as functions of known parameters such as the short-wave period, the angle of wave attack, the friction coefficient and the local wave height.

Notwithstanding that the main aim of the work is to clarify the structure of the SBCs for the longshore flow, derivation and assessment of such SBCs have been made on the basis of a fairly broad range of input wave conditions, which, though biased towards those typical of reflective beaches, are believed to cover conditions also typical of moderate dissipative beaches. Although the present calibration will probably to be further improved, we think that, as the experimental analyses of Archetti & Brocchini (2002) and of Bellotti *et al.* (2003) clearly show for the onshore SBCs, the range of its validity is broader than that covered by the input data used here.

We thank the Italian research institute INSEAN for partially supporting this study through the grant N. 798/PR. Thanks are also extended to Professor D. H. Peregrine, Professor T. E. Baldock and the three anonymous referees for the many useful comments and suggestions provided.

Appendix. Derivation of the regression equation (4.7)

A detailed derivation is here given of regression (4.7) used for $\mathfrak{B}(t)$ defined by (3.5) and (4.6).

First, use of (4.3), coming from Part 2, leads to:

$$\left.\begin{aligned} \langle \bar{u}\bar{v}d\rangle \approx (\sqrt{gH_l})(\sin(\theta)\sqrt{gH_l})H_l = A_1\sin(\theta)gH_l^2, \\ \langle \tilde{Q}_1\rangle = \langle \tilde{u}\tilde{d}\rangle \approx \sqrt{gH_l}H_l \\ \langle \tilde{Q}_2\rangle = \langle \tilde{v}\tilde{d}\rangle \approx \sqrt{gH_l}\sin(\theta)H_l \\ \langle \tilde{S}_{12}\rangle = \langle \tilde{u}\tilde{v}\tilde{d}\rangle \approx (\sqrt{gH_l})(\sin(\theta)\sqrt{gH_l})H_l = A_3\sin(\theta)gH_l^2, \end{aligned}\right\} \quad \Longrightarrow \frac{\langle \tilde{Q}_1\rangle\langle \tilde{Q}_2\rangle}{\bar{d}} = A_2 g H_l^2 \sin(\theta), \tag{A 1}$$

with A_i all constants.

Slightly more complicated is the derivation of the contribution depending on the velocity of the shoreline. However, recalling that from Part 2 it is $\langle V\rangle \approx H_l/\alpha$ and that the time scale is $\sqrt{H_l/g}/\alpha$ we easily obtain:

$$\left[\left(\bar{u} - \frac{\mathrm{d}x_l}{\mathrm{d}t}\right)\bar{v}\bar{d}\right]\Bigg|_{x_l} = -\left[\left(\frac{2}{H_l}\frac{\mathrm{d}\langle V\rangle}{\mathrm{d}t}\right)\bar{v}\bar{d}\right]\Bigg|_{x_l} \approx (\sqrt{gH_l})\bar{\bar{v}}H_l = A_4(\sqrt{gH_l})H_l\bar{\bar{v}}. \tag{A 2}$$

From a dimensional point of view, integration of $\mathfrak{B}$ in time merely means a multiplication by the mentioned time scale and, then, recalling (3.5) and (4.6):

$$\begin{aligned} \int_{t_k(y)}^{t} \mathfrak{B}(\tau, y)\,\mathrm{d}\tau &\approx \frac{1}{\alpha}\sqrt{\frac{H_l}{g}}\left[A_4\sqrt{gH_l}H_l\bar{\bar{v}} + \sin(\theta)gH_l^2(A_1 + A_2 + A_3 + A_5)\right] \\ &\approx \frac{H_l^2}{\alpha}[C_1\bar{\bar{v}} + C_2\sin(\theta)\sqrt{gH_l}], \end{aligned} \tag{A 3}$$

where A_5 accounts for the bottom friction contribution $\langle \Upsilon_2\rangle$ of equation (4.4*e*) and the constants C_i are used instead of A_i.

REFERENCES

Archetti, R. & Brocchini, M. 2002 An integral swash zone model with friction: an experimental and numerical investigation. *Coastal Engng* **45**, 89–110.

Baldock, T. E. & Holmes, P. 1999 Simulation and prediction of swash oscillations on a steep beach. *Coastal Engng* **36**, 219–242.

Baldock, T. E., Hughes, M. G., Day, K. & Louys, J. 2005 Swash overtopping and sediment overwash on a truncated beach. *Coastal Engng* **52**, 633–645.

Bellotti, G., Archetti, R. & Brocchini, M. 2003 Experimental validation and characterization of mean swash zone boundary conditions. *J. Geophys. Res. Oceans* **108**(C8), 3250, doi: 10.1029/2002JC001510.

Brocchini, M. 1997 Eulerian and Lagrangian aspects of the longshore drift in the surf and swash zones. *J. Geophys. Res. Oceans* **102**, 23 155–23 168.

Brocchini, M. 2006 Integral swash zone models. *Continent Shelf Res.* **26**, 653–660.

Brocchini, M. & Bellotti, G. 2002 Integral flow properties of the swash zone and averaging. Part 2. The shoreline boundary conditions for wave–averaged models. *J. Fluid Mech.* **458**, 269–281.

Brocchini, M. & Peregrine, D. H. 1996 Integral flow properties of the swash zone and averaging. *J. Fluid Mech.* **317**, 241–273.

Brocchini, M., Bernetti, R., Mancinelli, A. & Albertini, G. 2001 An efficient solver for nearshore flows based on the WAF method. *Coastal Engng* **43**, 105–129.

Elfrink, B. & Baldock, T. 2002 Hydrodynamics and sediment transport in the swash zone: a review and perspectives. *Coastal Engng* **45**, 149–167.

Kamphuis, J. W. 1991 Alongshore sediment transport rate distribution. *Coastal Sediments 91 Conference-ASCE*, vol. 1, pp. 170–183.

Longuet-Higgins, M. S. 1970 Longshore currents generated by obliquely incident sea waves, 1. *J. Geophys. Res. Oceans* **75**, 6778–6789.

Mase, H. 1995 Frequency down-shift of swash oscillations compared to incident waves. *J. Hydraul Res.* **33**, 397–411.

Masselink, G. & Puleo, J. A. 2006 Swash-zone morphodynamics. *Continent. Shelf Res.* **26**, 661–680.

Nielsen, P. 2002 Shear stress and sediment transport calculations for swash zone modelling. *Coastal Engng* **45**, 53–60.

Park, K.-Y. & Borthwick, A. G. L. 2001 Quadtree grid numerical model for nearshore wave–current interaction. *Coastal Engng* **42**, 219–239.

Russel, P. E. 1993 Mechanisms for beach erosion during storms. *Continent. Shelf Res.* **13**, 1243–1265.

Ryrie, S. C. 1983 Longshore motion generated on beaches by obliquely incident bores. *J. Fluid Mech.* **129**, 193–212.

Van Dongeren, A. R. & Svendsen, I. A. 2000 Non linear and quasi 3-D effects in leaky infragravity waves. *Coastal Engng* **41**, 467–496.

Van Wellen, E., Baldock, T. E., Chadwick, A. J. & Simmonds, D. 2000 Longshore sediment transport in the swash zone. *Proc. 27th Intl Conf. Coastal Engng ASCE*, vol. 1, pp. 3139–3150.

Wang, P., Ebersole, B. A., Smith, E. R. & Johnson, B. D. 2002 Temporal and spatial variations of surf-zone currents and suspended sediment concentration. *Coastal Engng* **46**, 175–211.

Zhao, Q. & Svendsen, I. A. 2006 Quasi-3d modeling of depth-averaged and depth-varying currents on a barred beach with a swash boundary condition. *Coastal Engng* (submitted).